Journal of Materials Chemistry A

PAPER

View Article Online
View Journal

Published on 17 October 2014. Downloaded by Heriot Watt University on 26/10/2014 09:46:54.

Cite this: DOI: 10.1039/c4ta04137b

Flexible interdigital-electrodes-based triboelectric generators for harvesting sliding and rotating mechanical energy†

Qiang Leng,‡ Hengyu Guo,‡ Xianming He, Guanlin Liu, Yue Kang, Chenguo Hu* and Yi Xi*

Received 11th August 2014
Accepted 24th September 2014

DOI: 10.1039/c4ta04137b

www.rsc.org/MaterialsA

Triboelectric generators have attracted considerable attention due to their rapidly improved electromechanical conversion efficiency. It is a great challenge to design a triboelectric generator to enable practical and effective operations. In this paper, we present a flexible interdigital-electrodes-based triboelectric generator (FITG) for harvesting sliding and rotating mechanical energy. When a film of flexible interdigital electrodes is placed on a plane, it can be used for harvesting sliding energy. When the film of the flexible interdigital electrodes is rolled into a cylinder, it can be used for harvesting rotating energy. In sliding mode, the maximum open-circuit voltage, short-circuit current and peak power density reach up to 400 V, 120 μA (10 mA m^{-2}) and 13 W m^{-2}, respectively, under a sliding velocity of 3.95 m s^{-1}, which can be used to light tens of light-emitting diodes (LEDs) and to charge a commercial capacitor to 7.2 V within 35 s. The FITG can harvest the mechanical energy of mouse operation and traditional printing. In rotating mode, the maximum output voltage of the generator reaches as high as 1020 V at a rotating speed of 240 rpm. The FITG with interdigital electrodes on a flexible substrate has the advantages of light weight, resistance to wear, multifunction and high output power.

Introduction

With the pursuit of a high-quality life and the rapid development of human society, energy is playing an increasingly important role in people's lives. As fossil energy is gradually being used up, it is urgent to search for green, renewable and sustainable energy resources. Harvesting energy from our ambient environment has attracted increasing attention for its extensive application in self-powered systems and small-scale energy needs.[1–3] In the past decade, various approaches for scavenging energy by using photovoltaic,[4–6] thermoelectric,[7–9] piezoelectric,[10–12] and triboelectric effects[13–17] have been widely investigated. Currently, the triboelectric nanogenerator based on electrification and the electrostatic induction effect is considered as one of the most promising methods because it can harvest almost any random mechanical energy including airflow,[18,19] vibration[20,21] and human motion.[22,23] To generate electricity, two triboelectric layers with opposite charges are made to contact and separate from each other under an external mechanical motion.[24] Recently, a TENG with two stationary electrodes and one free-standing triboelectric layer that moves in between under the guidance of an external mechanical motion has been developed. Furthermore, the electrode on the sliding part has been removed in a new design and a dielectric polymer layer can be inserted between the sliding part and the stationary electrodes, with which the TENG can significantly increase its lifetime and its energy conversion efficiency.[25–27] With a free-standing sliding part, this kind of triboelectric generator can avoid entanglement of the conducting wires connected on the electrodes when it works.

In the previous literature,[24,28] the output of a TENG is strictly associated with the effective periodic switching between charge contact and separation. If the switching interval could be greatly shortened, the output performance of the TENG would be markedly improved. Most of the previous generators are based on rigid electrodes, which make them not easy to assemble into a device system and realize multifunction. Therefore, generators based on flexible electrodes are needed to meet the requirements of self-powered electronic systems. In this paper, we design a flexible interdigital-electrode-based triboelectric generator (FITG) in which numerous stationary interdigital electrodes are fabricated on a flexible polyvinyl chloride (PVC) film that can be bent or folded at any angle and in any shape. As for each of the Al electrodes, several fingers connected in one are aligned in parallel. The FITG can work in two modes: one is sliding mode, and the other is rotating mode. For sliding mode, the film of flexible interdigital electrodes is flatly overlapped by one freestanding sliding panel with PTFE stripes on it, and,

Department of Applied Physics, Chongqing University, Chongqing 400044, P. R. China. E-mail: hucg@cqu.edu.cn; yxi6@cqu.edu.cn

† Electronic supplementary information (ESI) available. See DOI: 10.1039/c4ta04137b

‡ These authors contributed equally to this work.

Published on 17 October 2014. Downloaded by Heriot Watt University on 26/10/2014 09:46:54.

between the film of the electrodes and the sliding panel, sandwiched with a polyethylene terephthalate (PET) thin film. For rotating mode, the film of flexible interdigital electrodes is rolled into a cylinder and PTFE stripes on another cylinder are put inside the electrode cylinder, and between these coaxial cylinders also sandwiched with a PET thin film. The performance of the generator under different conditions, such as with different numbers of strips, at different sliding/rotating speeds, by different pressure on the sliding panel, with different thickness and type of the sandwiched dielectric layer, is investigated. In sliding mode, the maximum open-circuit voltage, short-circuit current and peak power density reach up to 400 V, 120 μA and 13 W m^{-2}, respectively, which can be used to light tens of light-emitting diodes (LEDs) and to charge a commercial capacitor to 7.2 V within 35 s. The FITG can harvest the mechanical energy of mouse operation and traditional printing. In rotating mode, the maximum output voltage of the generator reaches 1020 V at a rotating speed of 240 rpm. The FITG with interdigital electrodes on a flexible substrate has the advantages of light weight, resistance to wear, multifunction and high output power.

Experimental section

Fabrication of FITG for sliding mode

The structure of the FITG for sliding mode is shown in Fig. 1a, which illustrates two parts, the electrode part and sliding part. Fig. 1c shows a digital photograph of the FITG, demonstrating that the electrode part is flexible and can be bent into a cambered surface or rolled into a cylinder. The following are the fabrication methods of each part.

Electrode part. The electrode part is like a sandwich structure. In this experiment, a piece of commercial aluminium foil (width: 10 cm, length: 20 cm, thickness: 100 μm) was stuck on a piece of PVC film (width: 10 cm, length: 25 cm, thickness: 50 μm) for interdigital electrode fabrication. In the cutting process, the aluminium foil was carefully patterned to the interdigital electrodes (width of each electrode: 3 mm, interval between two electrodes: 1 mm) (Fig. 1a). After the cutting step, a PET or PVC film with various thicknesses (from 12.5 μm to 75 μm) was covered on the surface of the electrodes for comparative experiments.

Sliding part. The sliding part contains several PTFE strips (with surface inductively coupled plasma reactive ion etching treatment) (Fig. 1b) as electret material (100 μm) and an acrylic plate (thickness: 2 mm) as a substrate. The PTFE was cut to 3 mm in width and 4 cm in length for each piece, and stuck to an acrylic panel in parallel rows with an interval of 5 mm (Fig. 1c). The number of the strips varies from 1 to 15.

Fabrication of FITG for rotating mode

Electrode part. The sizes of the electrode film and electrode strips are 8 cm × 8.5 cm and 5 mm × 6 mm, respectively. The electrode film is rolled and attached onto the inside wall of the glass cylinder with a PET film covering its exposure surface as shown in Fig. 1d.

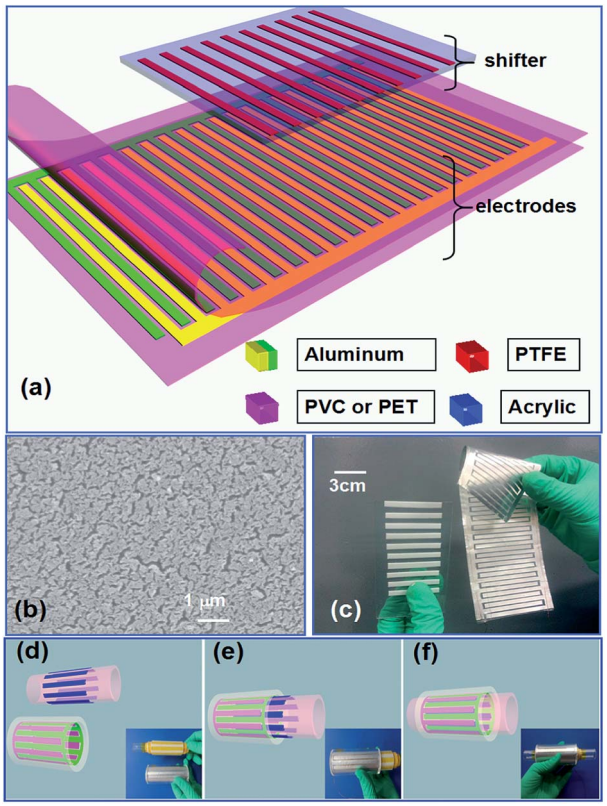

Fig. 1 (a) Schematic diagram of the FITG structure for sliding mode, including the sliding part and electrode part. (b) SEM image of the PTFE surface. (c) Digital photograph of FITG for sliding mode. (d)–(f) Schematic diagram of the fabrication of the FITG for rotating mode. The insets are the corresponding digital photographs of the real device in preparation steps.

Rotating part. Ten PTFE strips are stuck on the outside wall of another glass cylinder with a gap of 7 mm between two adjacent ones as shown in Fig. 1d. The PTFE strips are cut to 5 mm in width and 6 cm in length. The rotating part is inserted into the outer cylinder as depicted in Fig. 1e and f.

Characterization of FITG

The output performance of FITGs was measured using a Stanford low-noise current preamplifier (Model SR570) and a data acquisition card (NI PCI-6259). In sliding mode, the electrode part was fixed on a plate, while a linear motor (42HBS48BJ4-TR0) and a governor (ZD-6209-V2(C)) were used to produce motion with different frequencies of the sliding part with various weights on it, so that we can study the influence of speed and pressure on output performance. Fig. S1† schematically shows the measuring system.

In rotating mode, the electrode cylinder was fixed while the PTFE cylinder was driven to rotate by an electrical motor (51K40RA-D1500) with a digital display speed controller. The software Comsol Multiphysics based on finite-element simulation was employed to simulate the potential distribution in the FITG under open-circuit conditions.

 This journal is © The Royal Society of Chemistry 2014

Published on 17 October 2014. Downloaded by Heriot Watt University on 26/10/2014 09:46:54.

Results and discussion

Interdigital electrode structure

Each yellow or green electrode is connected at one end respectively to form interdigital electrodes as shown in Fig. 1a. The surface of the PTFE strips treated by ion etching is shown in Fig. 1b. The interdigital electrodes are quite flexible as shown in Fig. 1c, and can be folded in any shape. Moreover, this structure leads to excellent reliability and durability because the metal electrodes covered with PET/PVC thin film are not directly rubbed by the sliding panel.

Electricity generation process in sliding mode

The electricity produced by TENGs originates from mechanical motion through the coupling of triboelectrification and electrostatic induction: the periodic contact and separation of two different media with opposite charges change the induced potential difference across the two electrodes and thereby drive the alternating flow of electrons through an external load.[29–31] Fig. 2 presents the electricity generation process in sliding mode in detail. Fig. 2a shows the output current change during a whole sliding cycle. Because of the large difference in the ability to acquire electrons after being rubbed by each other, the PVC surface has a positive charge and the PTFE has a negative charge (see Fig. 2(b1)).[32] We define the initial state (Fig. 2(b1) and (f1)) or the final state (Fig. 2(d1)) when the electrode A (green) or electrode B (yellow) is overlapped by the PTFE strip. Fig. 2(c1) and (e1) represent the middle states where the sliding panel moves between the initial state and the final state.

To analyze the electricity-generating process, two light-emitting diodes (LEDs) are connected to the FITG. In the initial state, induced charges appear on electrode A (positive) and electrode B (negative) with equal charge density as illustrated in Fig. 2(b1). Without electron transfer, no current flows in the circuit, which can be evidenced by the unlighted LEDs in Fig. 2(b2). As the sliding panel moves from the state in Fig. 2(b1) to that in Fig. 2(d1), the charges on the electrode surface start to transfer. Free electrons flow from electrode B to A until the PTFE is in the final state (Fig. 2(d1)) where the charges reach a new equilibrium. Thus, there is a current flow from electrode A to B, which can be verified by lighting the left LED as shown in Fig. 2(c2) until it goes out (Fig. 2(d2)). As electrodes A and B are alternately aligned, in the next step, the sliding panel moves from electrode B to A (Fig. 2(e1)), while the free electrons flow from electrode A to electrode B until the sliding panel is in the initial state (Fig. 2(f1)). The current flows in reverse from electrode B to electrode A which drives the right LED lighting as shown in Fig. 2(e2) until it goes out (Fig. 2(f2)). In the whole cycle, the sliding panel moving from the electrode A group to the electrode B group and from the electrode B group to the electrode A group are symmetric; thus, a pair of symmetric alternating current peaks are observed, as depicted in Fig. 2a. The total charge transfer quantity and current can be expressed by the following equations[33,34]

$$Q = n\sigma l w(t),\ 0 \le w(t) \le w_0 \tag{1}$$

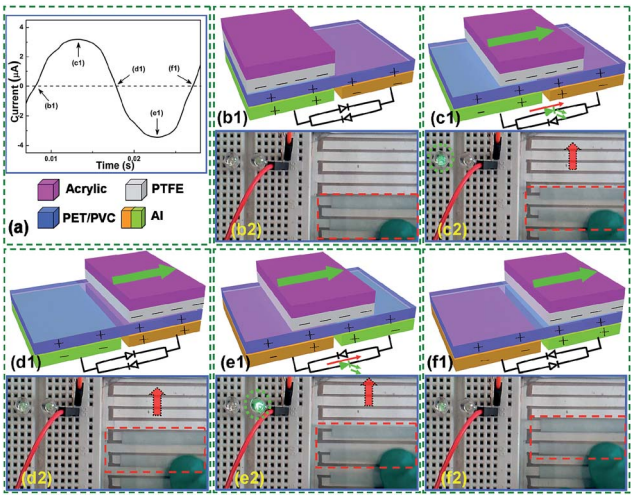

Fig. 2 Working mechanism of FITG in sliding mode. (a) The output current in a sliding cycle, (b1) electrode A is overlapped by one PTFE strip, (c1) the sliding panel moves from electrode A to B, (d1) electrode B is overlapped by PTFE, (e1) the sliding panel slides away from electrode B to A, (f1) initial state after a sliding cycle. (b2–f2) Corresponding photograph of each power process.

$$I = \frac{\mathrm{d}Q}{\mathrm{d}t} = n\sigma l \frac{\mathrm{d}w(t)}{\mathrm{d}t} = n\sigma l v \tag{2}$$

where n, σ, l and w_0 are the number of PTFE strips, the triboelectric charge density on the PTFE strips, and the length and width of a single PTFE strip, $w(t)$ is the displacement of the strips moving away from the initial state, and v is the sliding velocity of the sliding panel. To further study the process of electricity generation, we also simulate the potential difference between the two groups of interdigital electrodes at different times or states using COMSOL Multiphysics software (Fig. S2†).

Number of PTFE strips on sliding panel

The charge transfer quantity per unit time mainly determines the output current magnitude from eqn (2), while the quantity of charge on an electrode depends on the charge density of the PTFE strips and the total overlap area with the electrode from eqn (1). To investigate the influence of the overlapped area on the output current, we change the number of the PTFE strips. With an increase in the number of the strips, the output current increases correspondingly, as shown in Fig. 3a. The maximum output current can reach about 12 μA with 15 PTFE strips. As the PTFE strips are added, the area becomes larger and accordingly increases the total quantity of electric charge in accordance with eqn (1). From Fig. 3b, the total charge transfer quantity per second rises linearly as the number of PTFE strips increases, which consequently increases the output current.

Pressure on sliding panel

The contact tightness between the PTFE strips and the PVC film might affect the performance of the FITG. Therefore, different pressure is applied to the sliding panel with 5 PTFE strips. From

Published on 17 October 2014. Downloaded by Heriot Watt University on 26/10/2014 09:46:54.

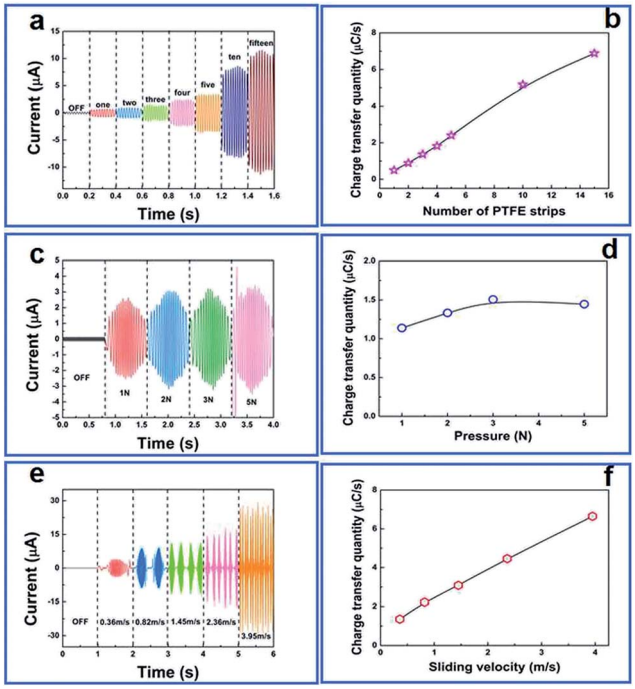

Fig. 3 Performance of FITG with sandwiched PVC film. (a) Output current with different numbers of PTFE strips on the sliding panel, and (b) corresponding charge transfer quantity. (c) Output current under different pressures, and (d) corresponding charge transfer quantity. (e) Output current under different sliding speeds, and (f) corresponding charge transfer quantity.

Fig. 3c, when no pressure is applied, the output current is quite low and is about 5 nA. After the pressure increases to 1 N, the value increases to 2.5 μA, much higher than the case without pressure. As the two triboelectric surfaces contact each other intimately with the pressure applied, the effective contact area increases owing to the nanostructure on the PTFE surface, which results in an increase in charge density on the PTFE film. However, as the pressure further increases from 2 N to 5 N, the output current seems to have achieved a saturation state. This is mainly because the PTFE strips and the PVC film have already contacted sufficiently. Higher pressure contributes little to the friction charge increase. As we can see from Fig. 3d, the charge transfer quantity increases with pressure in the beginning, then remains nearly constant later, which matches well with the change in output current.

Sliding velocity

The output current is proportional to the speed of the sliding panel according to eqn (2). To verify the influence of the sliding speed on the output, we systematically study the relationships between the output current, charge transfer quantity and sliding speed. We can obviously find that the output current increases with an increase in velocity, as shown in Fig. 3e. As for one PTFE strip, the charge transfer quantity per second per cycle remains unchanged (Fig. 3f). However, the amount of charge transfer per unit time becomes larger as the sliding speed increases.

Type of triboelectric layer

For triboelectric nanogenerators, the generation of electricity is based on the friction between two kinds of materials with different tendencies to gain or lose electrons in the triboelectrification process. To explore the influence of different types of triboelectric layers on the performance of the FITG, we choose another organic material, PET film, to conduct a comparative experiment. With the same number of PTFE strips, the output current with the PET film is larger, and the maximum value with 15 PTFE strips is 1.5 times larger than that with the PVC film, as shown in Fig. 4a. Under the same pressure and sliding speed, the performance of the FITG with the PET film is much better than that of the FITG with the PVC film, which can be seen from Fig. 4b and c. The maximum output current at the highest speed of 3.95 m s^{-1} almost doubles that with the PVC film. Compared with Fig. 3b, d and f, the corresponding charge transfers under the same conditions also match the tendency with the PVC film, as shown in Fig. 4d–f. The output current increase may be attributed to the difference in the tendency to gain or lose electrons between the PVC film and the PET film. Using PTFE and PET as the friction interface, high output power can be achieved due to the fact that PTFE has a strong tendency to gain electrons (negative charge) while PET has a strong tendency to lose electrons (positive charge). However, PTFE and PVC both have a tendency to lose electrons (negative charge) although PTFE has a higher negative charge tendency than that of PVC.[35] Therefore, less negative charge density is achieved using PTFE and PVC as friction interface. The lower charge density on

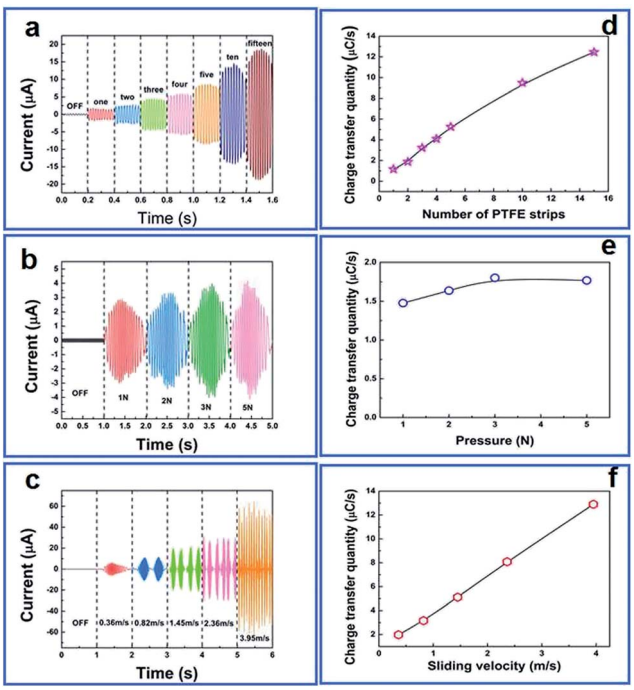

Fig. 4 Performance of FITG with PET film. (a) Output current with different numbers of PTFE strips on the sliding panel, and (d) corresponding charge transfer quantity. (b) Output current under different pressures, and (e) corresponding charge transfer quantity. (c) Output current under different sliding velocities, and (f) corresponding charge transfer quantity.

 This journal is © The Royal Society of Chemistry 2014

Published on 17 October 2014. Downloaded by Heriot Watt University on 26/10/2014 09:46:54.

PTFE film would result in a small output current based on eqn (2). As the FITG with a PET film can achieve a higher charge density, we choose PET film in the experiment below.

Thickness of the triboelectric layer

To investigate whether the thickness has an influence on the performance of the FITG, PET films with different thicknesses of 12.5 μm, 25.0 μm, 50.0 μm and 75.0 μm are sandwiched between the PTFE strips and the interdigital electrodes. As shown in Fig. 5a, with a thickness of 25.0 μm, the output current of the FITG achieves a maximum value of about 26 μA. However, as the thickness of the PET film increases, the output current gradually reduces to a minimum of 15 μA. PTFE is an electret and the negative charge on its surface will not change during the sliding process. Charge transfer is achieved only on the metal electrodes. As the charge transfer is driven by the electrostatic induction (electric potential difference) caused by the movement of the sliding panel, a thinner PET film would present a better driving force for the electron transfer. Therefore, it is better to choose thinner sandwiched triboelectric layers to induce efficient and rapid charge transfer between the electrodes to promote the performance of the FITG.

To evaluate the working efficiency of the FITG working in sliding mode, investigation of the output power with different external loads is indispensable. As displayed in Fig. 5b, the open-circuit voltage reaches 400 V with a load resistance of 700 MΩ. Fig. S3† shows the tendency of voltage at 700 MΩ. The current amplitude drops with an increase in load resistance while the voltage rises. Consequently, the peak power reaches a maximum at a load resistance of 2 MΩ as seen in Fig. 5c. The output power is calculated by the following equation:

$$P = I^2R$$

The calculation of the maximum output power value is shown in the ESI.† Moreover, to prove the durability of the device, a test is carried out after the device is rubbed three thousand times (see Fig. S4†).

Charging the commercial capacitor

For very small electronic devices, too high a voltage might not be safe and this prevents the FITG from powering them directly. Therefore, an energy storage unit is necessary to convert the high voltage to a working voltage, such as a capacitor or a battery.[36,37] A commercial capacitor (110 μF) is chosen for the charging test. Meanwhile, four light-emitting diodes (LEDs) in series are connected to the capacitor. Fig. 6a shows the charging

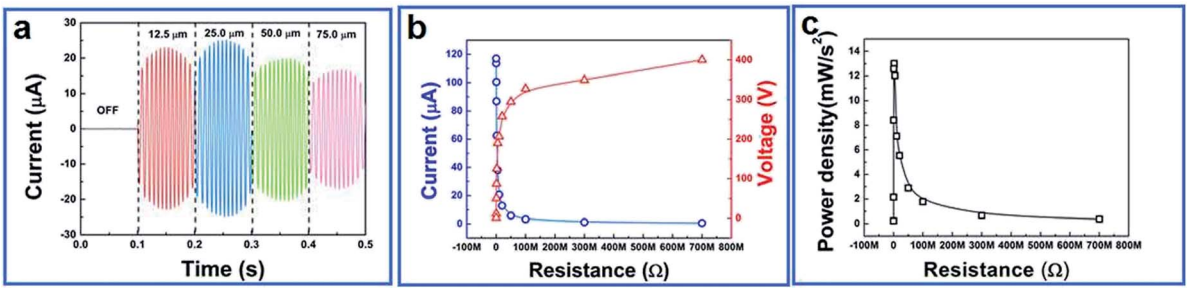

Fig. 5 (a) Output current under different thicknesses of the PET film. (b) Output current and voltage under different external loads. (c) Peak power under different external loads.

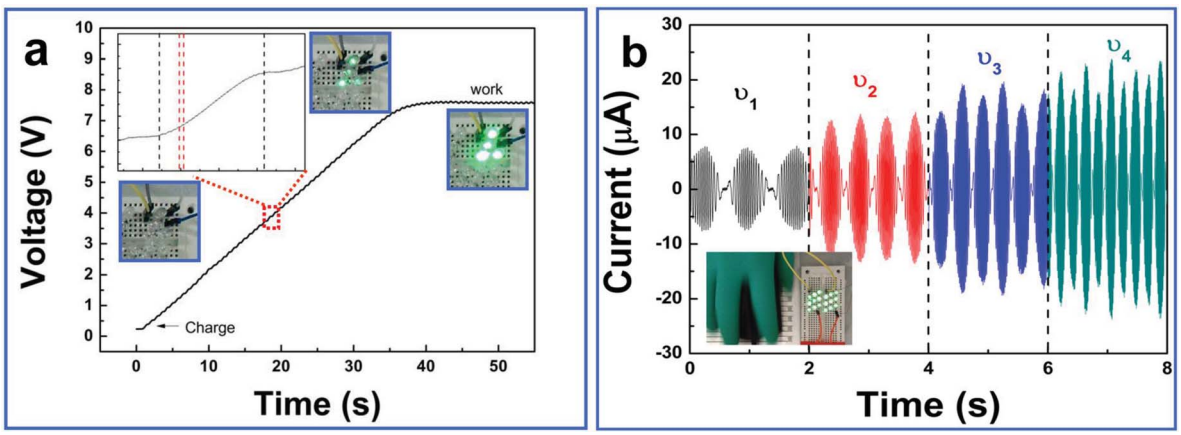

Fig. 6 (a) Voltage charging curve of the capacitor. The top left inset is the magnification of the voltage-time curve. The other three insets exhibit the whole process of charging and discharging of the capacitor. (b) The output current at different velocities of the mouse-based FITG. The velocity increases from *v*1 to *v*4. Inset shows the lit LEDs driven by the mouse motion.

Published on 17 October 2014. Downloaded by Heriot Watt University on 26/10/2014 09:46:54.

voltage-time curve, from which we can see that the capacitor is charged from 0 V to 7.5 V within 40 s. From the inset digital photograph, we can observe that the LEDs are off in the beginning due to the low electric energy charged in the capacitor. As the capacitor is charged more, the LEDs are gradually lighted to their maximum brightness. The top left inset is the magnification of the voltage-time curve. The steps in the plot correspond to the PTFE strips periodically moving toward and away from the electrodes. Video 1† shows the charging and discharging of the commercial capacitor.

Harvesting motion energy of computer mouse

Since personal computers have been popularized all around the world, as an indispensable part mice move constantly. It would be attractive to utilize the energy from the relative motion between the mouse and the mouse pad. Here, our flexible interdigital electrodes act as a mouse pad. Seven strips of PTFE are attached to the bottom of a computer mouse. As displayed in Fig. 6b, when we move the mouse back and forth slightly, an output current of ~5 μA is observed. When the motion accelerates, the output current increases correspondingly, which matches the results in Fig. 3e and 4c. Tens of LEDs can be lighted by moving the mouse, as shown in the inset, implying that simple mouse motion can generate considerable electric energy. Perhaps in the future, this mouse movement could help us to charge our electronic devices, such as mobile phones, while we are working or playing. Video 2† gives the whole working process of the mouse-based FITG.

Harvesting motion energy of traditional printing

After scaling up the sliding panel (about 4 times larger) and the interdigital electrodes (Fig. 7a), a traditional printing-based generator is fabricated, as shown in Fig. 7b. Moving the sliding panel forward and backward as in printing can generate quite a

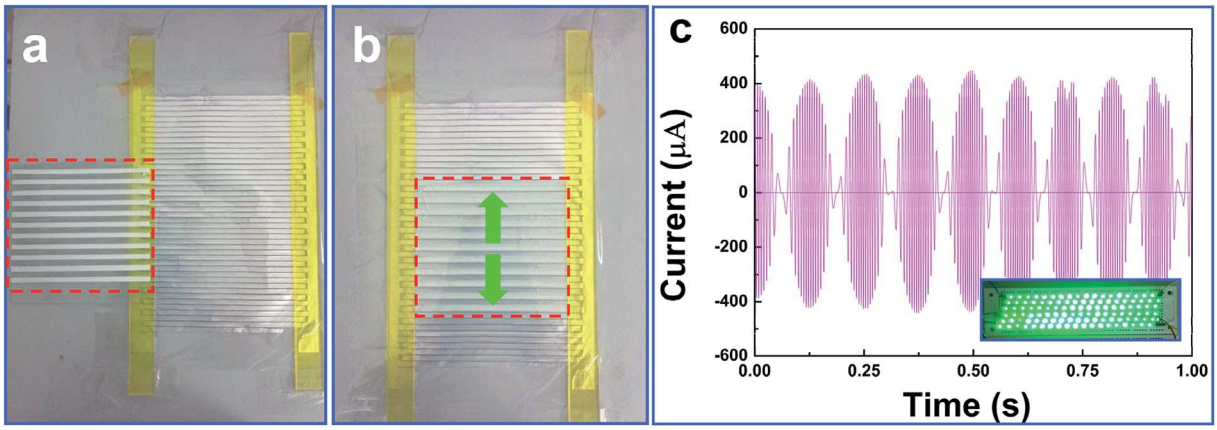

Fig. 7 (a) and (b) Structure of the traditional printing-based generator. (c) Output current of the generator. Inset is the photograph of the lit LEDs driven by the generator.

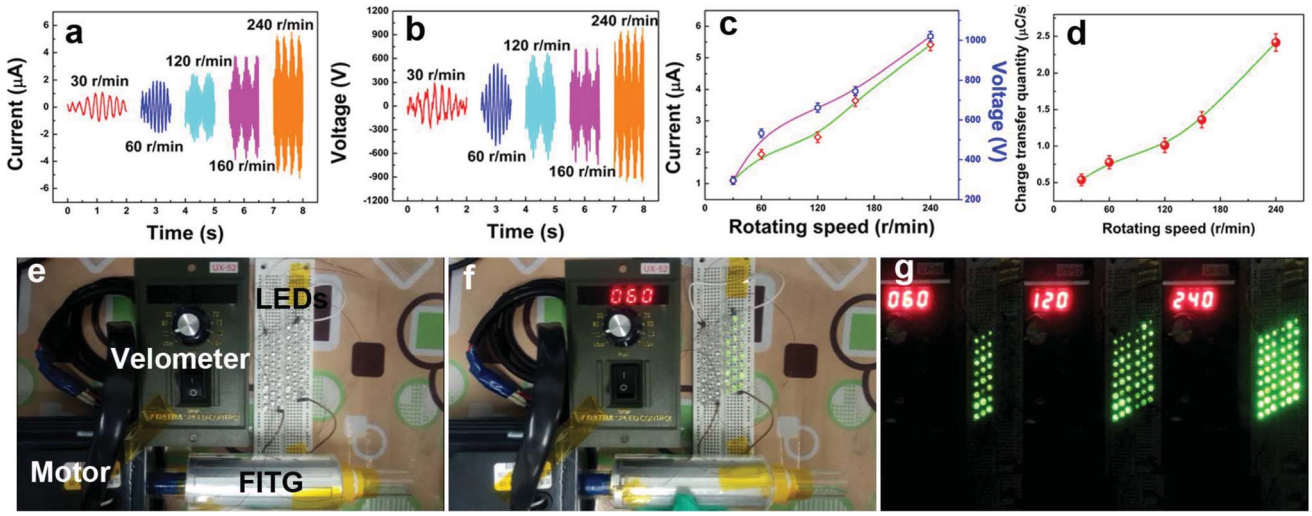

Fig. 8 (a) The output current and (b) open-circuit voltage of the FITG working at different rotating speeds. (c) The plots of current and voltage versus rotating speeds. (d) Charge transfer quantity of the FITG working at different rotating speeds. The photographs of (e) experimental setup and (f) working process and (g) the lit LEDs at different rotating speeds.

 This journal is © The Royal Society of Chemistry 2014

Published on 17 October 2014. Downloaded by Heriot Watt University on 26/10/2014 09:46:54.

considerable amount of electricity, which is depicted in Fig. 7c. The maximum output current of this generator can be as high as ~0.45 mA. Two rows of LEDs aligned in parallel are alternately lit up (inset). The brightness of these LEDs implies the high energy density output of our generator (see video 3†).

FITG working in rotating mode

For a triboelectric nanogenerator, the potential capacity to scavenge different kinds of mechanical energy becomes as important as its applications. Whether the generator can be applied extensively depends on whether the device can take advantage of different forms of ambient energy. To harvest rotating energy, the film of flexible interdigital electrodes is rolled into a cylinder and PTFE stripes on another cylinder are put inside the electrode cylinder, and between these coaxial cylinders is also sandwiched a PET thin film as shown in Fig. 1d–f. The output current and voltage increase with the increase in the rotating speed as shown in Fig. 8a–c. The maximum output voltage can reach about 1020 V. From Fig. 8d, the charge transfer quantities per second increase with the rotating speed. The detailed calculation method of the charge transfer quantity per unit time is illustrated in Fig. S5.† Fig. 8e and 8f show the photographs of experimental setup and working process. Through the brightness in Fig. 8g of the LEDs, the output power can be evaluated (see video 4†). Both the output current and voltage can be used to determine the rotating speed.

Conclusions

In summary, we have designed and fabricated flexible interdigital-electrodes-based triboelectric nanogenerators. The interdigital electrodes help shorten the cycle of charge transfer, thereby increasing the output current. The flexibility of the interdigital electrodes makes it possible to employ them to construct generators for harvesting sliding and rotating energy. In sliding mode, the FITG generates an open-circuit voltage of 400 V and a short-circuit current of 120 μA (10 mA m^{-2}) with a peak power of 13 W m^{-2} at a velocity of 3.95 m s^{-1}, which can drive tens of LEDs. The factors that influence the output current are elaborated, among which the number of the PTFE strips and the velocity of the sliding panel are proportional to the output current while the thickness of the triboelectric layer is inversely proportional to the output current. Moreover, the larger opposing tendency to gain/lose electrons between PTFE and the sandwiched film is effective in achieving higher output power. The produced electrical power can be used to charge commercial capacitors and light LEDs. The FITG can harvest the mechanical energy of mouse operation and traditional printing. In rotating mode, the maximum output voltage of the generator reaches as high as 1020 V at a rotating speed of 240 rpm. This investigation demonstrates that flexible interdigital electrodes can be used to construct multifunctional generators.

Acknowledgements

This work is supported by the NSFCQ (cstc2012jjB0006), SRFDP (20110191110034, 20120191120039), NSFC (11204388), the Fundamental Research Funds for the Central Universities (CDJRC10300001, CDJZR11300004, CDJZR12225501, CQDXWL-2013-012).

Notes and references

1 Y. Yang, H. L. Zhang, G. Zhu, S. Lee, Z. H. Lin and Z. L. Wang, *ACS Nano*, 2013, **7**, 785–790.
2 P. D. Mitcheson, E. M. Yeatman, G. K. Rao, A. S. Holmes and T. C. Green, *Proc. IEEE*, 2008, **96**, 1457–1486.
3 Z. L. Wang, G. Zhu, Y. Yang, S. H. Wang and C. F. Pan, *Mater. Today*, 2012, **15**, 532–543.
4 H. Kim, H. Jeong, T. K. An, C. E. Park and K. Yong, *ACS Appl. Mater. Interfaces*, 2013, **5**, 268–275.
5 E. G. Wang, L. T. Hou, Z. Q. Wang, S. Hellstrom, F. L. Zhang, O. Inganas and M. R. Andersson, *Adv. Mater.*, 2010, **22**, 5240–5244.
6 Y. H. Chen, W. C. Lin, J. Liu and L. M. Dai, *Nano Lett.*, 2014, **14**, 1467–1471.
7 Y. Du, K. F. Cai, S. Chen, P. Cizek and T. Lin, *ACS Appl. Mater. Interfaces*, 2014, **6**, 5735–5743.
8 D. Madan, Z. Q. Wang, A. Chen, R. C. Juang, J. Keist, P. K. Wright and J. W. Evans, *ACS Appl. Mater. Interfaces*, 2012, **4**, 6117–6124.
9 Y. Z. Pei, A. D. LaLonde, N. A. Heinz, X. Y. Shi, S. Iwanaga, H. Wang, L. D. Chen and G. J. Snyder, *Adv. Mater.*, 2011, **23**, 5674–5678.
10 Z. L. Wang and W. Z. Wu, *Angew. Chem., Int. Ed.*, 2012, **51**, 11700–11721.
11 S. Y. Xu, Y. W. Yeh, G. Poirier, M. C. McAlpine, R. A. Register and N. Yao, *Nano Lett.*, 2013, **13**, 2393–2398.
12 S. H. Shin, Y. H. Kim, M. H. Lee, J. Y. Jung and J. Nah, *ACS Nano*, 2014, **8**, 2766–2773.
13 J. J. Cole, C. R. Barry, R. J. Knuesel, X. Y. Wang and H. O. Jacobs, *Langmuir*, 2011, **27**, 7321–7329.
14 J. Henniker, *Nature*, 1962, **196**, 474.
15 Y. S. Zhou, Y. Liu, G. Zhu, Z. H. Lin, C. F. Pan, Q. S. Jing and Z. L. Wang, *Nano Lett.*, 2013, **13**, 2771–2776.
16 L. S. McCarty and G. M. Whitesides, *Angew. Chem., Int. Ed.*, 2008, **47**, 2188–2207.
17 Z. H. Lin, G. Cheng, L. Lin, S. M. Lee and Z. L. Wang, *Angew. Chem., Int. Ed.*, 2013, **125**, 12777–12781.
18 C. L. Sun, J. Shi, D. J. Bayer and X. D. Wang, *Energy Environ. Sci.*, 2011, **4**, 4508–4512.
19 Y. N. Xie, S. H. Lin, L. Wang, Q. S. Jing, Z. H. Lin, S. M. Niu, Z. Y. Wu and Z. L. Wang, *ACS Nano*, 2013, **7**, 7119–7125.
20 W. Q. Yang, J. Chen, G. Zhu, X. N. Wen, P. Bai, Y. J. Su, Y. Lin and Z. L. Wang, *Nano Res.*, 2013, **6**, 880–886.
21 S. P. Beeby, M. J. Tudor and N. M. White, *Meas. Sci. Technol.*, 2006, **17**, R175.
22 W. Q. Yang, J. Chen, G. Zhu, J. Yang, P. Bai, Y. J. Su, Q. S. Jing, X. Cao and Z. L. Wang, *ACS Nano*, 2013, **7**, 11317–11324.

Published on 17 October 2014. Downloaded by Heriot Watt University on 26/10/2014 09:46:54.

23 P. Bai, G. Zhu, Z. H. Lin, Q. S. Jing, J. Chen, G. Zhang, J. S. Ma and Z. L. Wang, *ACS Nano*, 2013, **7**, 3713–3719.
24 S. H. Wang, L. Lin and Z. L. Wang, *Nano Lett.*, 2012, **12**, 6339–6346.
25 S. H. Wang, Y. N. Xie, S. M. Niu, L. Lin and Z. L. Wang, *Adv. Mater.*, 2014, **26**, 2818–2824.
26 L. Lin, S. H. Wang, S. M. Niu, C. Liu, Y. N. Xie and Z. L. Wang, *ACS Appl. Mater. Interfaces*, 2014, **6**, 3031–3038.
27 H. Y. Guo, Q. Leng, X. M. He, M. J. Wang, J. Chen, C. G. Hu and Y. Xi, *Adv. Energy Mater.*, 2014, DOI: 10.1002/aenm.201400790.
28 L. Lin, S. H. Wang, Y. N. Xie, Q. S. Jing, S. M. Niu, Y. F. Hu and Z. L. Wang, *Nano Lett.*, 2013, **13**, 2916–2923.
29 Y. N. Xie, S. H. Wang, L. Lin, Q. S. Jing, Z. H. Lin, S. M. Niu, Z. Y. Wu and Z. L. Wang, *ACS Nano*, 2013, **7**, 7119–7125.
30 G. Zhu, C. F. Pan, W. X. Guo, C. Y. Chen, Y. S. Zhou, R. M. Yu and Z. L. Wang, *Nano Lett.*, 2012, **12**, 4960–4965.
31 G. Zhu, Z. H. Lin, Q. S. Jing, P. Bai, C. F. Pan, Y. Yang, Y. S. Zhou and Z. L. Wang, *Nano Lett.*, 2013, **13**, 847–853.
32 S. H. Wang, L. Lin, Y. N. Xie, Q. S. Jing, S. M. Niu and Z. L. Wang, *Nano Lett.*, 2013, **13**, 2226–2233.
33 C. Zhang, W. Tang, C. B. Han, F. R. Fan and Z. L. Wang, *Adv. Mater.*, 2014, **26**, 3580–3591.
34 G. Zhu, J. Chen, T. J. Zhang, Q. S. Jing and Z. L. Wang, *Nat. Commun.*, 2014, DOI: 10.1038/ncomms4426.
35 Z. L. Wang, *ACS Nano*, 2013, **7**, 9533–9557.
36 H. Y. Guo, X. M. He, J. W. Zhong, Q. Z. Zhong, Q. Leng, C. G. Hu, J. Chen, L. Tian, Y. Xi and J. Zhou, *J. Mater. Chem. A*, 2014, **2**, 2079–2087.
37 Q. Z. Zhong, J. W. Zhong, B. Hu, Q. Y. Hu, J. Zhou and Z. L. Wang, *Energy Environ. Sci.*, 2013, **6**, 1779–1784.

 This journal is © The Royal Society of Chemistry 2014